

Active MEMS metamaterials for THz bandwidth control

Kailing Shih, Prakash Pitchappa, Manukumara Manjappa, Chong Pei Ho, Ranjan Singh, Bin Yang, Navab Singh, and Chengkuo Lee

Citation: *Appl. Phys. Lett.* **110**, 161108 (2017); doi: 10.1063/1.4980115

View online: <http://dx.doi.org/10.1063/1.4980115>

View Table of Contents: <http://aip.scitation.org/toc/apl/110/16>

Published by the [American Institute of Physics](#)

Articles you may be interested in

[Controlling phase of microwaves with active graphene surfaces](#)
Appl. Phys. Lett. **110**, 161102161102 (2017); 10.1063/1.4980087

[Sensing with toroidal metamaterial](#)
Appl. Phys. Lett. **110**, 121108121108 (2017); 10.1063/1.4978672

[Silicon-immersed terahertz plasmonic structures](#)
Appl. Phys. Lett. **110**, 151105151105 (2017); 10.1063/1.4980018

[Dielectric metasurfaces for quantum weak measurements](#)
Appl. Phys. Lett. **110**, 161115161115 (2017); 10.1063/1.4982164

[Designing an efficient rectifying cut-wire metasurface for electromagnetic energy harvesting](#)
Appl. Phys. Lett. **110**, 083901083901 (2017); 10.1063/1.4976804

[Broadband metamaterial for optical transparency and microwave absorption](#)
Appl. Phys. Lett. **110**, 143511143511 (2017); 10.1063/1.4979543

Fearful for the future of science?

Sign up for **FREE** FYI emails.
AIP American Institute of Physics

Active MEMS metamaterials for THz bandwidth control

Kailing Shih,^{1,2,3,4} Prakash Pitchappa,^{1,2,4} Manukumara Manjappa,⁵ Chong Pei Ho,^{1,2,3,4} Ranjan Singh,⁵ Bin Yang,³ Navab Singh,⁶ and Chengkuo Lee^{1,2,4,7,a)}

¹Department of Electrical and Computer Engineering, National University of Singapore, Singapore 117576

²NUS Suzhou Research Institute (NUSRI), Suzhou, Industrial Park, Suzhou 215123,

People's Republic of China

³Department of Micro/Nano Electronics, Shanghai Jiao Tong University, Shanghai 200240,

People's Republic of China

⁴Center for Intelligent Sensors and MEMS (CISM), National University of Singapore, Singapore 117576

⁵Division of Physics and Applied Physics, Centre for Disruptive Photonic Technologies, School of Physical and New Mathematical Sciences, Nanyang Technological University, Singapore 637371

⁶Institute of Microelectronics (IME), 11 Science Park Road, Singapore 117685

⁷Graduate School for Integrative Science and Engineering, National University of Singapore, Singapore 117456

(Received 12 January 2017; accepted 2 April 2017; published online 19 April 2017)

We experimentally demonstrate a microelectromechanical system (MEMS) based metamaterial with actively tunable resonance bandwidth characteristics, operating in the terahertz (THz) spectral region. The broadband resonance characteristic feature of the MEMS metamaterial is achieved by integrating sixteen microcantilever resonators of identical lengths but with continuously varying release lengths, to form a supercell. The MEMS metamaterial showed broadband resonance characteristics with a full width half maximum (FWHM) value of 175 GHz for resonators with a metal thickness of 900 nm and was further improved to 225 GHz by reducing the metal thickness to 500 nm. The FWHM resonance bandwidth of the MEMS metamaterial was actively switched to 90 GHz by electrostatically controlling the out-of-plane release height of the constituent microcantilever resonators. Furthermore, the electrically controlled resonance bandwidth allows for the active phase engineering with relatively constant intensity at a given frequency based on the reconfiguration state of the MEMS metamaterial. This enables a pathway for the realization of actively controlled transmission or reflection based on dynamically programmable THz metamaterials. *Published by AIP Publishing.*

[<http://dx.doi.org/10.1063/1.4980115>]

Electromagnetic (EM) metamaterials are arrays of sub-wavelength structures, which have been shown to have interesting EM properties, such as artificial magnetism,¹ negative refractive index,² wavelength selective absorption,³ narrow band emission,⁸ classical analogue of electromagnetically induced transparency (EIT),^{4–7} Fano resonance,⁹ and many more. The disruptive feature of metamaterials comes from the possibility of achieving varied EM properties by engineering the unit cell geometry. However, most of these reported metamaterials are limited to provide a narrow band response, which greatly hinder their usage from applications desiring broadband characteristics such as broadband cloaking, imaging, and spectrometry. Few earlier reports on broadband resonance metamaterials realized this by integrating multiple overlapping narrow band resonators into one supercell.^{10–17} The constituent resonators in the supercell are either placed in a planar configuration with a lateral spatial variation¹⁵ or stacked on top of one another.¹⁶ Alternatively, multiple modes of the complex resonator design such as nested split ring resonators are also reported to achieve broadband resonance.¹⁴ The planar broadband metamaterial is easier to fabricate but provides lower resonance strength due to the reduced number of resonators in a given area. On the other hand, the stacked resonator metamaterial is more difficult to fabricate but provides stronger resonance strength. However, either of these

broadband resonance metamaterials reported so far are usually passive or can achieve active amplitude modulation of broadband resonance.¹⁸ The active tunability of the resonance bandwidth in terahertz (THz) metamaterials is yet to be reported and will be a critical component in the realization of dynamic bandwidth allocation for bandwidth control in next generation sub-THz wireless communication systems.

The active control of the metamaterial response is of immense importance for the realization of various metadevices, which will enable numerous practical applications.¹⁹ Conventionally, the active control of the metamaterial response is achieved by integrating active materials into the resonator geometry or as a surrounding medium, whose properties can be controlled through external stimulus such as optical,^{20,21} electrical,²² thermal,^{23,24} and magnetic fields.²⁵ However, the use of active materials over the wide spectral range is limited due to their frequency dependent material properties, complexity in the fabrication process, and need for bulky systems to provide the external control. Alternatively, structural reconfiguration of the resonator geometry by integrating microelectromechanical system (MEMS) based microactuators has been reported as an efficient means of achieving tunable metamaterials especially in THz^{18,26–32} and infrared^{33–35} spectral regions. In recent years, MEMS metamaterials have been reported for the active control of numerous EM properties such as magnetic response,^{27,36} electrical response,^{32,37} multiband switching,^{38,39} EIT analogue,^{40–42} phase engineering,⁴³ and

^{a)} Author to whom correspondence should be addressed. Electronic mail: elc@nus.edu.sg

chirality.⁴⁴ Versatility of the microactuator design, ease of process integration, and electrical control makes it an ideal candidate for realizing high performance and miniaturized metadvice systems.

In this paper, we experimentally demonstrate a MEMS metamaterial with electrostatically tunable bandwidth characteristics operating in the THz spectral region. The MEMS metamaterial supercell consists of 4×4 arrays of cantilever dipolar resonators of identical total length ($60 \mu\text{m}$) and width ($5 \mu\text{m}$) but with gradually varying release lengths. This allows for the realization of the broadband response in the initial OFF state, when no voltage is applied. When voltage is applied between the released cantilever and silicon substrate, the out-of-plane gap is closed, and all sixteen cantilevers resonate at the same resonance frequency, leading to a narrow band response in the ON state. The proposed MEMS metamaterial with bandwidth tunability can be adopted in realization of next generation THz wireless communication channels, THz imaging, and spectroscopic applications.

The proposed broadband MEMS metamaterial supercell consists of an array of sixteen cantilever resonators with gradually varying release lengths (Fig. 1(a)). The cantilever has fixed part of length l_f and released part of length l_r , which are made of bimaterial layers— t_{Al} the thickness of aluminum (Al) on top of t_{d} the thickness of aluminum oxide (Al_2O_3) (Fig. 1(b)). The cantilever with no release part is termed as C1, and on the other hand, the cantilever that is completely released is termed as C16. All other cantilevers C2–C15 have gradually varying released lengths with a step value of $4 \mu\text{m}$. The optical microscopy image of sixteen cantilever resonators is shown in Fig. 1(c). The released part of the cantilever is bent in the out-of-plane direction with the tip displacement (g), which is due to the residual stress in the bimaterial layers.^{30,45} When THz waves with an electric field aligned along the cantilever length is incident on the metamaterial formed with a single cantilever as a unit cell, narrow dipolar resonance is achieved.³⁷ The resonance frequency of the cantilever metamaterial is given by $f_r \sim (L_{\text{eff}} \cdot C_{\text{eff}})^{-1/2}$, where L_{eff} and C_{eff} are the effective inductance and capacitance of the cantilever resonator, respectively. C_{eff} is a series

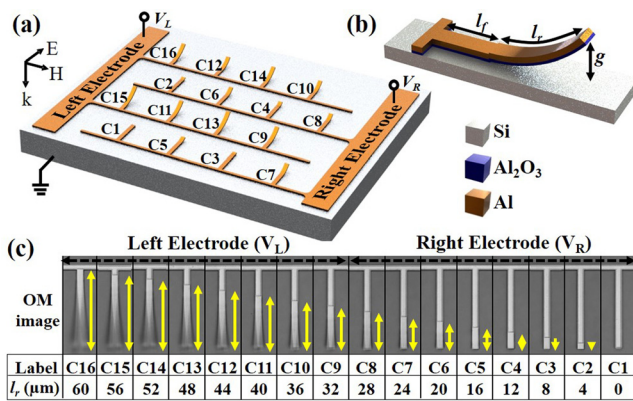


FIG. 1. (a) Schematics of a bandwidth tunable MEMS metamaterial supercell formed by a 4×4 array of microcantilever resonators with varying fixed and released lengths. (b) Schematic of a microcantilever resonator with geometrical definitions. (c) Optical microscopy image of the fabricated microcantilever resonators (C1–C16) with varying fixed and released lengths.

combination of capacitance from the Al_2O_3 layer (C_d) and out-of-plane gap (C_g), i.e., $C_{\text{eff}} \propto (C_d \cdot C_g)/(C_d + C_g)$. The out-of-plane gap capacitance is given by $C_g \propto (l_r \cdot w_c)/g$, and so based on the values of l_r and g , the cantilever dipolar resonance can be engineered accordingly. Even with cantilever resonators of equal total length, the dipolar resonances can be altered by exploiting the third dimension of metamaterial design to achieve overlapping resonance bands that can be integrated to enable planar broadband resonance metamaterials.

The effects of l_r and g on the f_r of the cantilever resonators were independently studied by finite difference time domain (FDTD) modeling. The out-of-plane gap is quantified in the simulations by using a parameter termed as release angle, $\theta = \sin^{-1}(g/l_r)$. First, metamaterials with a single cantilever resonator at fixed θ and varying l_r were studied. The simulated THz transmission spectra of the cantilever metamaterials at $\theta = 1^\circ$ and varying l_r are shown in Fig. 2(a). The dipolar resonance frequency of C1 ($f_{r,C1}$) was observed at 0.58 THz. As l_r increases, the corresponding f_r redshifts gradually and the narrowest band f_r is achieved for C16 ($f_{r,C16} = 0.705$ THz). Hence, by integrating all sixteen cantilevers into a supercell, broadband resonance can be achieved by the superposition of sixteen dipolar resonances (dashed curve in Fig. 2(a)). The maximum resonance frequency shift between the cantilevers forming a supercell is calculated as $\Delta f = f_{r,C16} - f_{r,C1}$. It is also important to note that the resonance strength decreases

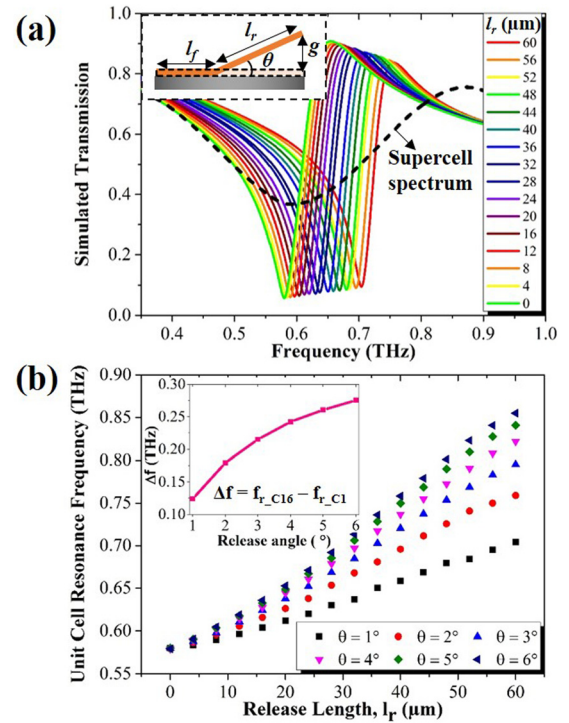


FIG. 2. (a) Simulated microcantilever metamaterial THz transmission spectra with varying release lengths, l_r , at a release angle of $\theta = 1^\circ$. The black dashed line shows the Lorentz fitted broadband resonance spectrum of the supercell formed by combining all sixteen microcantilever unit cells with varying l_r into a single supercell, and the inset shows the geometrical definitions of l_r , δ , and θ . (b) Simulated microcantilever resonator based metamaterial THz transmission spectra with varying l_r and θ . The inset shows the calculated maximum resonance frequency shift between microcantilever resonators with minimum $l_r = 0 \mu\text{m}$ (C1) and maximum $l_r = 60 \mu\text{m}$ (C16) as $\Delta f = f_{r,C16} - f_{r,C1}$ at varying θ .

with increasing l_r due to reduced electric field confinement in the out-of-plane gap. Furthermore, simulations were carried out for varying θ from 1° to 6° (Fig. 2(b)). Since θ_{C1} is always 0° , the $f_{r,C1}$ remains unchanged. However, for the other cantilevers, the increment of f_r at any given l_r decreases with increasing θ . This is because of the large out-of-plane gap between the cantilever and substrate, leading to weaker resonances at the higher frequency range in the unit cell.^{37,39} The Δf was calculated for $\theta = 1^\circ$ to 6° and is shown in the inset of Fig. 2(b). The Δf for $\theta = 6^\circ$ is calculated to be 0.275 THz, which is 120% higher than that for the $\theta = 1^\circ$ case with 0.175 THz. Furthermore, the saturating behavior of Δf at higher values of θ is clearly observed. This defines the maximum bandwidth that is achievable in the MEMS metamaterial. Hence, from the simulation results, it is obvious that the proposed approach of selectively releasing a part of the cantilever provides an added dimensionality for the realization of broadband resonance metamaterials.

The proposed broadband MEMS metamaterial was fabricated using a CMOS compatible process ($t_{Al} = 900$ nm; $t_d = 50$ nm)³² with $100 \mu\text{m}$ pitch between cantilevers in an area of 1 cm^2 (supplementary material). Sixteen cantilevers are positioned in a manner to have certain differences in the release length with their neighboring resonators, thus preventing undesired sequential effects as a super cell. The eight cantilevers with shorter l_r (C1–C8) were electrically connected to each other but isolated from the metal lines connecting the other eight cantilevers with larger l_r (C9–C16). This electrical isolation allows for the independent actuation of two sets of cantilevers to enable advanced control of the resonance bandwidth. When voltage is applied between the Al layer of cantilevers and the substrate, the electrostatic force pulls the released cantilevers towards the substrate. After a particular value of input voltage called pull-in voltage, the cantilevers will come in contact with the substrate.^{46,47} This allows for the active control of the gap capacitance C_g of the MEMS metamaterial, and hence its resonance frequency can be controlled with greater precision. The voltage applied to shorter and longer l_r cantilevers is termed as V_R and V_L , respectively.

The THz transmission response of the fabricated reconfigurable broadband MEMS metamaterial was measured using a THz-time domain spectrometry (THz-TDS) system with THz waves incident normally on the sample and electric field polarized along the cantilever length. The THz transmission amplitude and phase of the MEMS metamaterial at various reconfiguration states are shown in Figs. 3(a) and 3(b), respectively. When $V_R = V_L = 0$ V, the cantilevers are suspended with varying l_r and g , and hence broadband resonance is observed. This experimentally verifies the proposed concept of realizing broadband resonance in the THz metamaterial by MEMS technology. As V_R is selectively increased, the shorter l_r cantilevers move towards the substrate and blueshifts the corresponding resonance frequencies. The resonance strength increases in the lower frequency range due to the increased number of resonators (C2–C8) with f_r close to $f_{r,C1}$. This increased asymmetry in the cantilever resonance frequency variation causes a slight increase in the overall resonance bandwidth of the MEMS metamaterial. More importantly, when V_L is increased, strong reduction in the resonance bandwidth can be observed. This is due to the significantly larger change in the out-of-plane gap capacitance of C9–C16. When $V_R = V_L = 40$ V, all the sixteen cantilevers are identical with no gap below. This leads to a single narrow band resonance at 0.58 THz. Due to the increased number of resonators, the narrow band resonance strength is also significantly higher. The full-width half maximum bandwidth (B) of the measured THz spectra is determined by fitting the curve with the Lorentzian function and deducing the B value. The B of the MEMS metamaterial, when $V_L = V_R = 0$ V, was measured to be 0.175 THz and was tuned to a narrow B equal to 0.09 THz (Fig. 3(c)). The transmission phase (φ) was also measured at various reconfiguration states (Fig. 3(b)). When the resonance bandwidth was larger, the phase gradient ($d\varphi/df$) was lower, and as the bandwidth reduces, the phase gradient gets sharper (Fig. 3(c)). Hence, the resonance bandwidth tunability indirectly enables the control of phase gradient. More interestingly, the change in the phase gradient can be engineered to achieve specific phase values with relatively constant

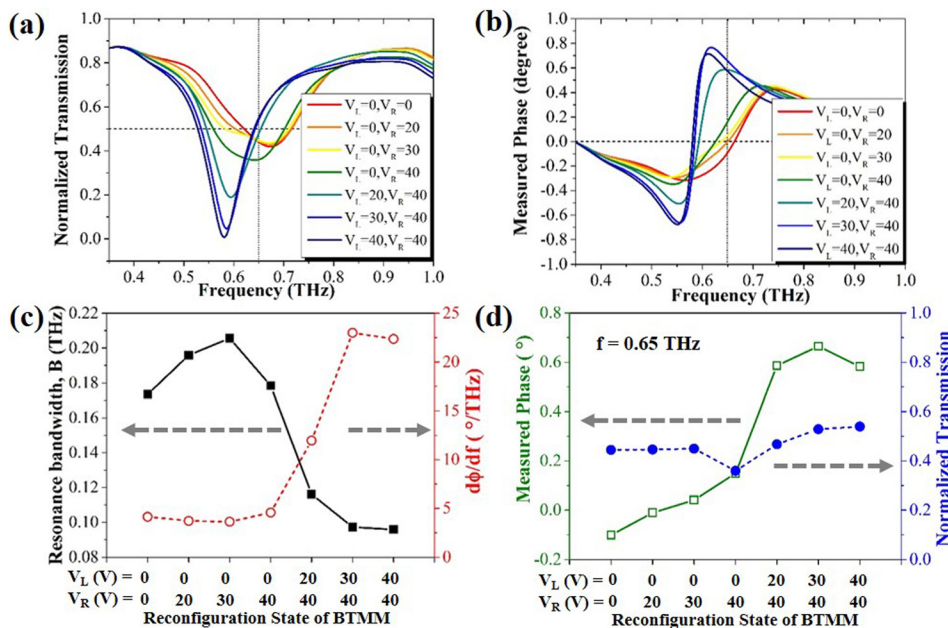


FIG. 3. Measured (a) THz transmission and (b) phase of the bandwidth tunable MEMS metamaterial (BTMM) with a metal thickness of 900 nm in various reconfiguration states. (c) Measured FWHM resonance bandwidth, B (black-solid curve), and phase change gradient, $d\varphi/df$ (red-dash curve) in various reconfiguration states of the BTMM. (d) Measured THz transmission (blue-dash curve) and phase (green-solid) at 0.65 THz in various reconfiguration states of the BTMM.

amplitude and can potentially be used as dynamically programmable meta-bits in coding metamaterials.⁴⁸ The measured phase change and normalized transmission at 0.65 THz in various reconfiguration states are shown in Fig. 3(d). Although the phase change observed here is very small for practical applications, the proposed design approach can be adopted in a metal-insulator-metal configuration to achieve larger and more accurate phase control.⁴³

In order to experimentally study the θ variation, two other samples were fabricated with lower t_{Al} of 700 nm and 500 nm. The three fabricated samples with $t_{\text{Al}} = 900$ nm, 700 nm, and 500 nm are termed as D900, D700, and D500, respectively. The tip displacement (g) of all the cantilevers for the three fabricated samples were measured using a reflection digital holographic microscope. The measured g strongly depends on the value of t_{Al} as shown in Fig. 4(a).³⁷ The g increases with increasing l_r and reducing t_{Al} . Unlike the consideration made in the simulations, the values of both l_r and θ vary at the same time in real devices. The increase in g of the cantilever with decreasing t_{Al} is primarily caused due to the reduction in spring constant of the cantilevers. Hence, in experiments, the influence of θ is studied by varying t_{Al} .³⁷ All three MEMS metamaterials were characterized for their THz transmission response in various reconfiguration states. The B value of the transmission spectra are shown in Fig. 4(b). For D700, when $V_R = V_L = 0$ V, the B value is measured to be 0.225 THz, which is approximately 75% higher than that of D900 ($B = 0.175$ THz). This confirms that the B of the MEMS metamaterial increases with

increasing θ . Compared to the D900 sample, a similar trend of bandwidth tuning is observed in the case of D700. When $V_L = V_R = 40$ V, the resonance bandwidth of D700 was measured to be 0.09 THz, which matches with that of D900 in the same reconfiguration state. In this state, all the cantilevers are identical since they are all in physical contact with the substrate. The only difference between D700 and D900 is t_{Al} , which has negligible influence on their resonance frequencies and corresponding bandwidths. More interestingly, in the case of D500 when $V_L = V_R = 0$ V, the resonance bandwidth is measured to be 0.225 THz, which is identical to that of D700. Although, the g of all the cantilevers for D500 is higher than that of D700, the resonance strength of the cantilevers especially with larger l_r becomes extremely weak and hence does not contribute to the resonance broadening effect.³⁹ This experimentally shows the saturating behavior of the increasing resonance bandwidth with larger θ values as predicted in the simulations. However, the trend of resonance bandwidth tuning with the same order of reconfiguration states is identical to all three samples. For D500 when $V_L = V_R = 40$ V, the B was approximately 123 GHz, which is higher than that of both D700 and D900. This could be caused due to the higher voltage required for completely closing the out-of-plane gap for cantilevers with larger g . By increasing the applied voltage, the bandwidth of the D500 can also be narrowed to 90 GHz. Although in simulation, the effects of l_r and θ are studied independently, in the real case, their variations mutually depend on each other. This leads to the slight difference between the simulated and measured THz transmission spectra. Furthermore, the saturating resonance broadening can be overcome by varying the total length of cantilevers, which is not explored here. The proposed approach of the achieving broadband THz response using the MEMS metamaterial can also be adopted for the realization of spectral broadband switching, polarization-insensitive tunable bandwidth systems, and broadband tunable absorbers that would enable a wide range of potential THz applications.

In summary, a broadband MEMS metamaterial with an electrically tunable bandwidth is experimentally demonstrated by integrating cantilever resonators of varying release lengths into one supercell. The measured FWHM of 0.175 THz was achieved, which was reduced to 0.09 THz. The broadband resonance width was further increased by 120% by reducing the Al thickness from 900 nm to 700 nm. However, with a further reduction in the Al thickness to 500 nm, no obvious resonance broadening was observed. These MEMS metamaterials are fabricated using the CMOS compatible process and can be easily integrated to application specific to ICs to enable electrical control signaling. A similar approach can be applied to metamaterial resonator designs and hence can enable the whole class of interesting THz properties with a broadband spectral response. This makes the proposed MEMS metamaterial to be an ideal candidate for realization of numerous miniaturized broadband THz systems and a critical component for bandwidth management in next generation sub-THz wireless communication systems.

See [supplementary material](#) for a detailed description of the simulation method, the sample preparation, and the device performance.

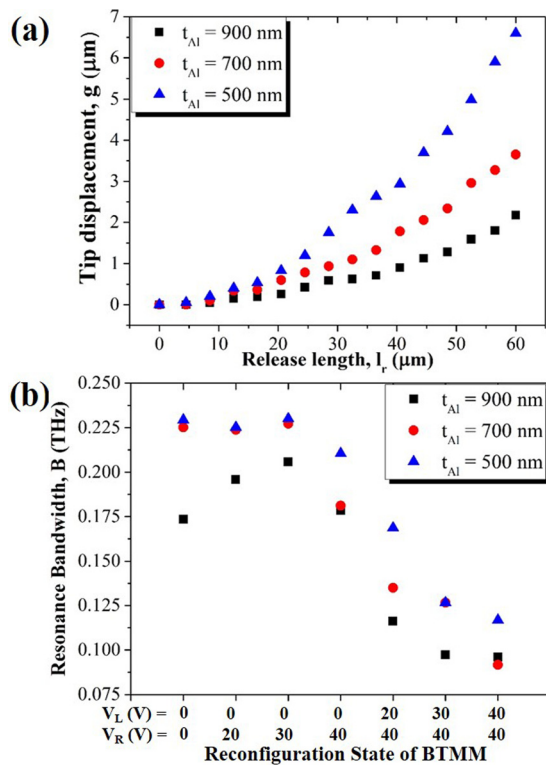


FIG. 4. (a) Measured tip displacement of the bandwidth tunable MEMS metamaterials—D900 (black-square), D700 (red-circle), and D500 (blue-triangle), respectively. (b) Measured FWHM resonance bandwidth of D900 (black-square), D700 (red-circle), and D500 (blue-triangle) at various reconfiguration states.

The authors acknowledge the financial support from the research grant (No. NRF-CRP001-019) at the National University of Singapore and partially supported by the National Natural Science Foundation of China under Grant No. 61474078 at the NUS (Suzhou) Research Institute, Suzhou, China. M.M. and R.S. acknowledge the research funding support from NTU startup Grant No. M4081282, Singapore, MOE Grant Nos. M4011362, MOE2011-T3-1-005, and MOE2015-T2-2-103.

- ¹J. B. Pendry, A. J. Holden, D. Robbins, and W. Stewart, *IEEE Trans Microwave Theory Tech.* **47**, 2075 (1999).
- ²R. A. Shelby, D. R. Smith, and S. Schultz, *Science* **292**, 77 (2001).
- ³N. Landy, S. Sajuyigbe, J. Mock, D. Smith, and W. Padilla, *Phys. Rev. Lett.* **100**, 207402 (2008).
- ⁴R. Singh, C. Rockstuhl, F. Lederer, and W. Zhang, *Phys. Rev. B* **79**, 085111 (2009).
- ⁵P. Tassin, L. Zhang, T. Koschny, E. Economou, and C. M. Soukoulis, *Phys. Rev. Lett.* **102**, 053901 (2009).
- ⁶M. Manjappa, S.-Y. Chiam, L. Cong, A. A. Bettiol, W. Zhang, and R. Singh, *Appl. Phys. Lett.* **106**, 181101 (2015).
- ⁷M. Manjappa, Y. K. Srivastava, and R. Singh, *Phys. Rev. B* **94**, 161103 (2016).
- ⁸X. Liu, T. Tyler, T. Starr, A. F. Starr, N. M. Jokerst, and W. J. Padilla, *Phys. Rev. Lett.* **107**, 045901 (2011).
- ⁹R. Singh, I. A. Al-Naib, Y. Yang, D. R. Chowdhury, W. Cao, C. Rockstuhl, T. Ozaki, R. Morandotti, and W. Zhang, *Appl. Phys. Lett.* **99**, 201107 (2011).
- ¹⁰J. Han, J. Gu, X. Lu, M. He, Q. Xing, and W. Zhang, *Opt. Express* **17**, 16527 (2009).
- ¹¹Y. Q. Ye, Y. Jin, and S. He, *JOSA B* **27**, 498 (2010).
- ¹²S. Gu, J. Barrett, T. Hand, B.-I. Popa, and S. Cummer, *J. Appl. Phys.* **108**, 064913 (2010).
- ¹³N. Han, Z. Chen, C. Lim, B. Ng, and M. Hong, *Opt. Express* **19**, 6990 (2011).
- ¹⁴D. R. Chowdhury, R. Singh, M. Reiten, H.-T. Chen, A. J. Taylor, J. F. O'Hara, and A. K. Azad, *Opt. Express* **19**, 15817 (2011).
- ¹⁵S. Gu, B. Su, and X. Zhao, *J. Appl. Phys.* **114**, 163702 (2013).
- ¹⁶F. Ding, Y. Jin, B. Li, H. Cheng, L. Mo, and S. He, *Laser Photonics Rev.* **8**, 946 (2014).
- ¹⁷L.-H. Gao, Q. Cheng, J. Yang, S.-J. Ma, J. Zhao, S. Liu, H.-B. Chen, Q. He, W.-X. Jiang, and H.-F. Ma, *Light: Sci. Appl.* **4**, e324 (2015).
- ¹⁸M. Unlu and M. Jarrahi, *Opt. Express* **22**, 32245 (2014).
- ¹⁹N. I. Zheludev and Y. S. Kivshar, *Nat. Mater.* **11**, 917 (2012).
- ²⁰H.-T. Chen, J. F. O'Hara, A. K. Azad, A. J. Taylor, R. D. Averitt, D. B. Shrekenhamer, and W. J. Padilla, *Nat. Photonics* **2**, 295 (2008).
- ²¹M. Manjappa, Y. K. Srivastava, L. Cong, I. Al-Naib, and R. Singh, *Adv. Mater.* **29**, 1603355 (2017).
- ²²H.-T. Chen, W. J. Padilla, J. M. Zide, A. C. Gossard, A. J. Taylor, and R. D. Averitt, *Nature* **444**, 597 (2006).
- ²³Q.-Y. Wen, H.-W. Zhang, Q.-H. Yang, Y.-S. Xie, K. Chen, and Y.-L. Liu, *Appl. Phys. Lett.* **97**, 021111 (2010).
- ²⁴R. Singh, A. K. Azad, Q. Jia, A. J. Taylor, and H.-T. Chen, *Opt. Lett.* **36**, 1230 (2011).
- ²⁵L. Kang, Q. Zhao, H. Zhao, and J. Zhou, *Opt. Express* **16**, 8825 (2008).
- ²⁶H. Tao, A. Strikwerda, K. Fan, W. Padilla, X. Zhang, and R. Averitt, *Phys. Rev. Lett.* **103**, 147401 (2009).
- ²⁷W. M. Zhu, A. Q. Liu, X. M. Zhang, D. P. Tsai, T. Bourouina, J. H. Teng, X. H. Zhang, H. C. Guo, H. Tanoto, and T. Mei, *Adv. Mater.* **23**, 1792 (2011).
- ²⁸W. Zhu, A. Liu, W. Zhang, J. Tao, T. Bourouina, J. Teng, X. Zhang, Q. Wu, H. Tanoto, and H. Guo, *Appl. Phys. Lett.* **99**, 221102 (2011).
- ²⁹W. Zhu, A. Liu, T. Bourouina, D. Tsai, J. Teng, X. Zhang, G. Lo, D. Kwong, and N. Zheludev, *Nat. Commun.* **3**, 1274 (2012).
- ³⁰Z. Han, K. Kohno, H. Fujita, K. Hirakawa, and H. Toshiyoshi, *Opt. Express* **22**, 21326 (2014).
- ³¹C. P. Ho, P. Pitchappa, Y.-S. Lin, C.-Y. Huang, P. Kropelnicki, and C. Lee, *Appl. Phys. Lett.* **104**, 161104 (2014).
- ³²F. Ma, Y.-S. Lin, X. Zhang, and C. Lee, *Light: Sci. Appl.* **3**, e171 (2014).
- ³³X. Liu and W. J. Padilla, *Adv. Opt. Mater.* **1**, 559 (2013).
- ³⁴P. Pitchappa, C. P. Ho, P. Kropelnicki, N. Singh, D.-L. Kwong, and C. Lee, *Appl. Phys. Lett.* **104**, 201114 (2014).
- ³⁵N. I. Zheludev and E. Plum, *Nat. Nanotechnol.* **11**, 16 (2016).
- ³⁶Z. Han, K. Kohno, H. Fujita, K. Hirakawa, and H. Toshiyoshi, *IEEE J. Sel. Top. Quantum Electron.* **21**, 2700809 (2015).
- ³⁷P. Pitchappa, C. P. Ho, L. Dhakar, Y. Qian, N. Singh, and C. Lee, *J. Microelectromech. Syst.* **24**, 525 (2015).
- ³⁸P. Pitchappa, C. P. Ho, L. Dhakar, and C. Lee, *Optica* **2**, 571 (2015).
- ³⁹P. Pitchappa, C. P. Ho, Y. Qian, L. Dhakar, N. Singh, and C. Lee, *Sci. Rep.* **5**, 11678 (2015).
- ⁴⁰P. Pitchappa, M. Manjappa, C. P. Ho, R. Singh, N. Singh, and C. Lee, *Adv. Opt. Mater.* **4**, 541 (2016).
- ⁴¹P. Pitchappa, M. Manjappa, C. P. Ho, Y. Qian, R. Singh, N. Singh, and C. Lee, *Appl. Phys. Lett.* **108**, 111102 (2016).
- ⁴²P. Pitchappa, M. Manjappa, C. P. Ho, R. Singh, N. Singh, and C. Lee, *Appl. Phys. Lett.* **109**, 211103 (2016).
- ⁴³L. Cong, P. Pitchappa, Y. Wu, L. Ke, C. Lee, N. Singh, H. Yang, and R. Singh, *Adv. Opt. Mater.* **5**, 1600716 (2017).
- ⁴⁴T. Kan, A. Isozaki, N. Kanda, N. Nemoto, K. Konishi, H. Takahashi, M. Kuwata-Gonokami, K. Matsumoto, and I. Shimoyama, *Nat. Commun.* **6**, 8422 (2015).
- ⁴⁵Y.-S. Lin, Y. Qian, F. Ma, Z. Liu, P. Kropelnicki, and C. Lee, *Appl. Phys. Lett.* **102**, 111908 (2013).
- ⁴⁶Y. Qian, L. Lou, M. J. Tsai, and C. Lee, *Appl. Phys. Lett.* **100**, 113102 (2012).
- ⁴⁷P. Singh, C. G. Li, P. Pitchappa, and C. Lee, *Electron Device Lett., IEEE* **34**, 987 (2013).
- ⁴⁸T. J. Cui, M. Q. Qi, X. Wan, J. Zhao, and Q. Cheng, *Light: Sci. Appl.* **3**, e218 (2014).